Fabricating Customizable 3-D Printed Pressure Sensors by Tuning Infill Characteristics

Jiakun Yu, Praneeth Bimsara Perera, *Member, IEEE*, Rahal Viddusha Perera, Mohammad Mirkhalaf Valashani, and Anusha Withana

***Abstract*—We present a novel method for fabricating customizable pressure sensors by tuning the infill characteristics of flexible 3-D prints, addressing the demand for precise sensing solutions across a range of applications requiring variable softness. This article investigates the properties of infill patterns and densities on the mechanical behavior of 3-D prints using both computational simulation and empirical data. We demonstrate how Young's modulus of the 3-D prints can be systematically altered through infill parameters, enabling the creation of sensors with customized responses. In addition, we identify several infill patterns that are better suited for specific applications: *Gyroid* patterns for omnidirectional force at lower softness, *Grid* patterns for unidirectional force at moderate softness, and *Isolated* patterns for higher softness. Our findings indicate that higher infill densities generally align more closely with theoretical predictions, offering more reliable sensor behavior. We used the results to create an intuitive graphical user interface as a design tool, which not only facilitates the precise modification of a sensor's sensitivity and dynamic range but also suggests parameters to enhance printing quality for specific softness. Finally, we exhibit the versatility of this method through the fabrication of sensors for three exemplar applications with different sensing needs.**

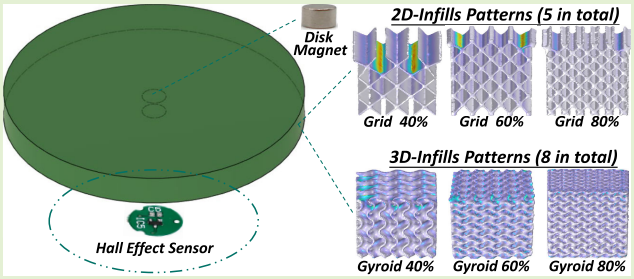

***Index Terms*— Customization, fabrication, finite element analysis, pressure sensor.**

Manuscript received 17 December 2023; revised 11 January 2024; accepted 11 January 2024. Date of publication 31 January 2024; date of current version 14 March 2024. The works of Mohammad Mirkhalaf Valashani and Anusha Withana were supported by the Australian Research Council Discovery Early Career Award, through the Australian Government under Grant DE200100479 and Grant DE210100975. This work was supported by the Neurodisability Assist Trust, Australia, and DSI, University of Sydney. The associate editor coordinating the review of this article and approving it for publication was Dr. Wensong Wang. *(Corresponding author: Jiakun Yu.)*

This work involved human subjects or animals in its research. Approval of all ethical and experimental procedures and protocols was granted by the University of Sydney's Human Research Ethics Committee under Application No. 2019/553.

Jiakun Yu is with the School of Computer Science, The University of Sydney, Sydney, NSW 2006, Australia (e-mail: jiakun.yu@sydney.edu.au).

Praneeth Bimsara Perera and Rahal Viddusha Perera are with the School of Computer Science, The University of Sydney, Sydney, NSW 2006, Australia, and also with the Department of Electronics and Telecommunication Engineering, University of Moratuwa, Moratuwa 10400, Sri Lanka (e-mail: praneeth.perera@sydney.edu.au; rahal.perera@sydney.edu.au).

Mohammad Mirkhalaf Valashani is with the School of Mechanical, Medical, and Process Engineering, Queensland University of Technology, Brisbane, QLD 4000, Australia (e-mail: mohammad.mirkhalaf@qut.edu.au).

Anusha Withana is with the School of Computer Science and the Sydney Nano Institute (Sydney Nano), The University of Sydney, Sydney, NSW 2006, Australia (e-mail: anusha.withana@sydney.edu.au).

Digital Object Identifier 10.1109/JSEN.2024.3358330

I. Introduction

CUSTOMIZED physical devices add significant value to different applications, especially for users with unique needs. For instance, in rehabilitation, the customization within end-user development (EUD) of devices plays a pivotal role in assisting patients with conditions such as stroke or multiple sclerosis [1]. For instance, low-temperature thermoplastics (LTTPs) are commonly used to create smart orthoses due to their flexibility and the ease of incorporating electronics, which enables better alignment with the body [2]. Furthermore, research shows that custom 3-D printed items can enhance security issues, such as two-factor authentication, in digital services [3]. To this end, recent research shows a great promise in utilizing 3-D printing to facilitate customization [4], [5], [6], [7].

Three-dimensional printing, with its rapid prototyping, cost-effectiveness, and material reusability, has enhanced various human-computer interaction (HCI) sensing applications including touch [8], [9], hover [10], [11], press [12], [13], twist [14], [15] and tilt [16], [17]. Its adaptability in creating responsive objects with changeable geometries has further extended sensing interfaces [9], [11], [18]. Additionally, the exploration of innovative fabrication techniques [19], [20], [21], [22] and diverse materials with electrical [10],

[23], photochromic [24], [25], thermochromic [26], [27], and magnetic functionalities [28], [29], [30] has broadened the scope of sensory capabilities.

Unlike methods requiring building extra features [9], [31], [32], our method leverages an integral role of 3-D printing: infills. While infills are typically employed for supportive structure [33], [34], [35], in our method, they serve as compressible architecture essential for modifying mechanical behaviors in sensor applications. This novel use of infills, leveraging their inherent properties in 3-D printing, has not been extensively explored for sensing purposes.

In this article, we proposed a methodology to fabricate customizable pressure sensors by tuning the infill patterns and densities. Different infill patterns have their unique physical characteristics. By adjusting these patterns and their density, we can give 3-D printed objects different mechanical properties. We first used simulations to illustrate how changes in these parameters affect mechanical properties such as Young's modulus, and the distribution of maximum strain and stress within a 3-D model, providing a theoretical foundation for our approach. Subsequently, we use empirical results to show how the concept can be realized in 3-D printed objects. The effectiveness of our approach is assessed by creating three exemplar applications that detect deformation by embedding magnets and Hall effect sensors. Additionally, we have developed an easy-to-use design tool to facilitate end users.

In summary, this article is presented as follows.

1) An approach to 3-D printing easily customizable pressure sensors by adjusting infill parameters.
2) A simulation and empirical data-driven design tool for customizing sensor sensitivity and dynamics.
3) Concept demonstrations using exemplar applications.

II. Related Work

In this section, we will discuss the current literature on the mechanical properties of customizable interfaces and 3-D printing infill architectures.

A. Mechanical Properties of Customizable Interfaces

In HCI, customizable interfaces refer to devices or systems adaptable in form and function, facilitating tailored user interactions. This field has seen significant advancements through mechanical techniques, known for their rapid prototyping and iterative design. For instance, Olberding et al. [36] and Yamaoka et al. [37] developed foldable, shape-changing devices using printed electronics. Weigel et al. [38] and Kao et al. [39] broadened the user scenarios for on-body touch surfaces using flexible and stretchable materials. Additionally, Ion et al. [40] explored the use of 3-D printing to create objects with customized stiffness and directional strength. They introduced a concept where the internal microstructure of materials is engineered to achieve specific mechanical functions, a field known as metamaterials. In our research, we take this concept further by using infill—a fundamental aspect of 3-D printing—as a type of metamaterial. This approach simplifies the design and production of interactive mechanical interfaces, capitalizing on the ease of modifying infill patterns in standard 3-D printing software.

Moreover, the ability to tune mechanical properties is crucial for enhancing sensor functionality. For example, MyoSpring [41] demonstrated this by using 3-D printed springs in wrist-worn sensors for precise finger movement detection. Flexibles [8] showed how altering the placement of embedded electrodes in 3-D prints can lead to different types of deformation sensing. Our work contributes to this field by examining how the compressibility of infill influences the sensitivity and dynamic range of pressure sensors. This has significant potentials for applications like full-range human motion monitoring [42], [43] and the development of self-powered pressure sensors [44].

B. 3-D Printing Infill Architecture

Infill architecture in 3-D printing defines the internal structure of a printed object. Its design plays a crucial role in optimizing material usage, part strength, and overall printing time. Existing literature has explored how altering the architecture and concentration of material within the infill can influence the mechanical properties of the printed object [33], [34], [35]. Such studies have shown that varying infill parameters influence both tensile [33] and compressive [34] strengths under perpendicular force.

While these studies offer insights into selecting appropriate infills, their primary focus remains on the rigidity and strength of the 3-D print. In contrast, the potential of infill as an influential factor in the mechanical user interface is comparatively less explored. In this article, instead of emphasizing the supportive function of the infill, our research brings a fresh perspective by exploring the compressibility aspect of the infill. In sensing modality, some works have touched upon manipulating infill density to modify sensor sensitivity, equating such changes essentially as area alterations in fiber Bragg grating [45], [46] and electrodes [47]. However, the broader implications of varying infill patterns and densities for magnetic sensing in deformable sensors remain unexplored.

III. Infill Design: From Supportive to Compressible Architectures

We used the open-source slicing tool, Ultimaker Cura,[1] for adjusting infill parameters. It provides more infill options than alternatives and it is freely accessible.

A. Understanding and Categorizing Infills

Infills are conventionally used as internal supportive structures in 3-D printing. It ensures that the shape is preserved during and post-printing, especially vital when the design has overhangs or flat areas prone to deformation. Moreover, infill allows material conservation and reduction in printing time by creating hollow models without compromising structural integrity. Formed in repeated patterns like Grids or Gyroids, the density of infill can vary, offering great customization

[1] https://ultimaker.com/software/ultimaker-cura

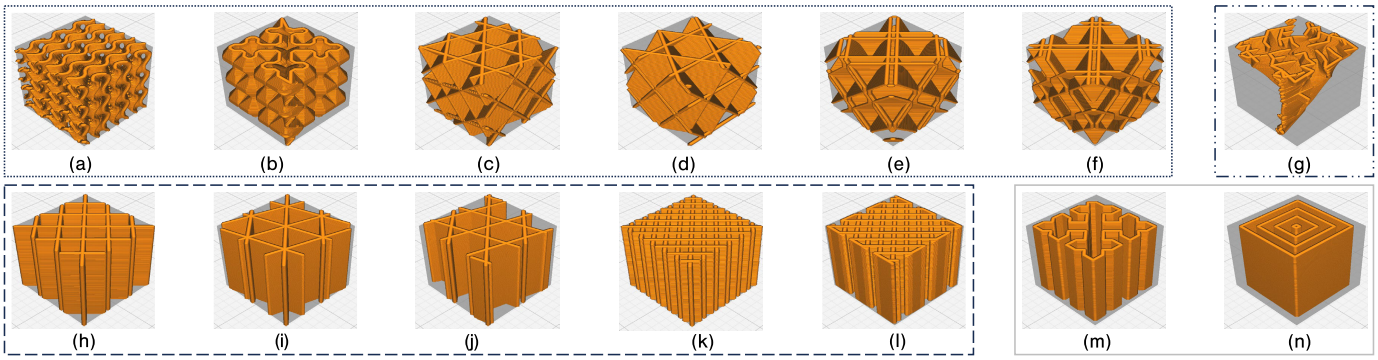

Fig. 1. Illustration of infill patterns. (a)–(f) Variations of 3-D infills (gyroid, cross 3-D, cubic, cubic subdivision, quarter cubic, and octet, respectively). (h)–(l) Types of conventional 2-D infills (grid, triangles, tri-hexagon, lines, and zig zag, respectively). (g) Visually purposed infill pattern. (m) and (n) Examples of Isolated 2-D infills, all at an infill density of 40%.

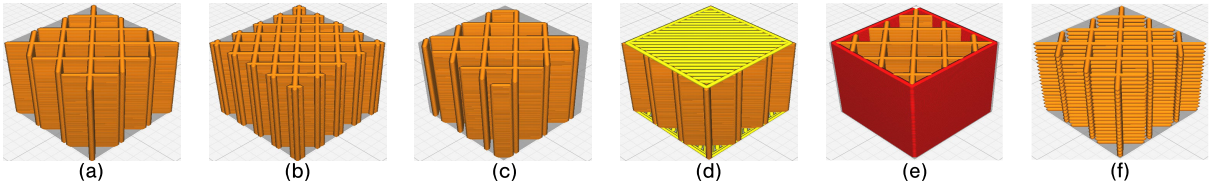

Fig. 2. (a) Baseline: 40% infill density, 0.2 mm layer height, no offset, wall, or top and bottom layers. (b)–(f) Other Parameters: (b) 60% Infill Density, (c) 5mm X-Offset, (d) Top/Bottom Layers, (e) Wall, (f) 0.5mm Layer Height.

potential to control the printed part's weight, strength, and flexibility.

1) Types of Infill Patterns: Fig. 1 showcases commonly used infill patterns in 3-D printing. These can be broadly categorized into 2-D and 3-D patterns. 2-D patterns, like *Grids*, are supportive vertically but compressible horizontally (In the orientation of Fig. 1). Some 2-D patterns, such as *Concentric*, produce isolated areas, which we term as *Isolated 2-D infill patterns*. On the other hand, 3-D patterns, such as *Gyroids*, often inspired by biology [35], provide consistent strength in all directions, making them ideal for objects under varied stresses. Lightning infill is a fast-printing irregular geometry that primarily supports the top surfaces of the printed object and is usually wrapped by outside peripherals for esthetic purposes. The choice of pattern largely depends on the specific application. Apart from the visual-oriented *Lightning* infill, patterns are typically classified as either 3-D or 2-D.

2) Infill Parameters: There are several changeable parameters besides patterns in infills. First, the *density*, also referred to as volume concentration [Fig. 2(b)], indicates the amount of material filling an object's interior. A higher density leads to a stronger but heavier object, while a lower density leads to a lighter and potentially flexible one. We utilize it as a means to modulate Young's modulus of objects.

Other parameters such as X or Y offset, illustrated in Fig. 2(c), determines how the infill aligns with the direction of the applied force. Surrounding this, the top-bottom layers and wall parameter, showcased in Fig. 2(d) and 2(e), serve as an enclosing boundary, providing protective surfaces for the infill, ensuring the infill remains shielded from external factors. Moreover, the layer height, depicted in Fig. 2(f), defines the quality of the printed infill structure. However, while these parameters are instrumental in shaping the infill's overall design and printing quality, they do not directly dictate its mechanical properties. It's the infill densities and patterns that have a more pronounced influence on the rigidity of the infill, as emphasized by Samykano et al. [48].

3) Filaments: In 3-D printing, not every material or filament is easily deformable. Standard filaments like polylactic acid (PLA) and acrylonitrile butadiene styrene (ABS) proved hard to deform in our early tests. Therefore, we opted for a thermoplastic polyurethane (TPU) filament, NinjaFlex,[2] due to its high deformability in printed samples. It features a density (ρ) of 1190 kg/m^3, a Young's modulus (E) of 1.2×10^7 Pa, and a Poisson's ratio of 0.48 [49]. We used these characteristics in our simulations.

B. Simulation of Compressible Architectures

Several related works have quantitatively analyzed infills when used for support [33], [34]. However, the concept of employing infills as compressible architectures remains less explored. To bridge this gap, we conducted simulation studies on 13 commonly used 2-D and 3-D infills, focusing on their compressible behaviors. The aim was to gather quantitative data on their compressibility across three infill densities: 40%, 60%, and 80%.

Our simulations utilized the solid mechanics physics tool in COMSOL multiphysics. The range of forces was kept the same for all infill patterns, maintaining conditions within the bilinear strain region. For 2-D models, the force was applied parallel to the patterns, as deformation is more likely to occur in that direction. For 3-D models, we applied vertical forces, given that deformations are comparable in both lateral

[2]https://ninjatek.com/shop/ninjaflex/

and perpendicular directions. From the resulting deformations, we calculated Young's modulus to obtain our quantitative data.

For simulation, we created 10 mm cubes GCODE for each infill pattern and density using *Cura*. Then they were subsequently regenerated, repaired, and improved by voxelizer,[3] Fusion 360 and SolidWorks respectively. This conversion procedure from STL to GCODE and then back to STL ensures that the simulated models are the same as printed models.

C. Sensing Principle

To effectively measure pressure levels, we evaluated various sensing mechanisms for capturing deformations. Piezo and resistive pressure sensors, while initially considered, were found to be prone to hysteresis and inconsistency [50], [51], [52]. Additionally, IMUs offer precision but require complex circuitry and additional electrical connectivity [53], [54], [55]. Capacitive sensing was also explored; however, it proved less effective for large deformations due to its need for small electrode ranges [56], [57]. Consequently, we chose magnetic sensing, specifically Hall effect sensors, for their longer sensing range, high bandwidth, lower power consumption, and lack of interference from body proximity [58], [59], [60], [61], [62]. This magnetic sensing approach is integrated with the unique properties of 3-D print infill in our model, which is designed for vertical printing to ensure compressibility. During the printing process, we pause midway to place a disk magnet within the structure, as depicted in Fig. 3(a), enhancing the seamless integration between the magnet and infills.

As illustrated in Fig. 3(b), the deformable structure is sandwiched between a thin disk magnet at the top and a Hall effect sensor at the bottom. The variation of magnetic flux density (ΔB) of a disk magnet with radius (R), thickness (D), and Remanence field (B_r) on its symmetry axis at a gap z can be approximated as below [63], [64]

$$\Delta B \approx \frac{B_r}{2}\left(\frac{\Delta z}{\sqrt{R^2+(D+z)^2}} - \frac{\Delta z}{\sqrt{R^2+z^2}}\right). \quad (1)$$

In our sensor design, it is important to maintain the sensor within the elastic region to avoid irrecoverable deformation. This necessitates limiting compression distances in the z-direction, which is reflected in the small compression distance (Δz) in the equation. Deformation here alters the gap z between the magnet and sensor, causing a change in the magnetic flux density (ΔB), which is proportional to the Δz. This relationship can be further expressed in terms of the Young's modulus (E) of the architecture as below [63], [65]

$$\Delta F = EA\left(\frac{\Delta z}{Z}\right) \propto \Delta B. \quad (2)$$

By adjusting the internal architecture, such as the infill, we can influence Young's modulus (E). For instance, lower infill densities decrease the architecture's porosity and, consequently, its elastic modulus.

[3]https://zmorph3d.com/software/

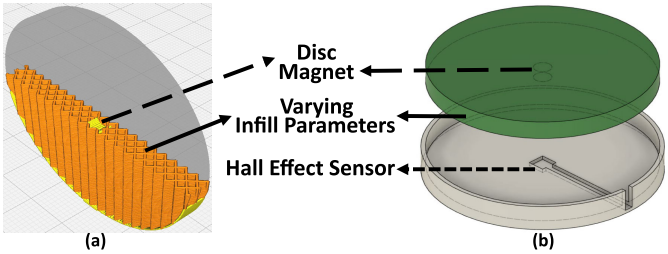

Fig. 3. Concept of sensing. (a) Cross-sectional view midway through the print. (b) Locations of disk magnetic sensors and Hall effect sensors.

IV. Results for Simulation and Experiments

A. Simulation Result

Using COMSOL's solid mechanic interface for a stationary study, we assessed the impact of varying infill patterns and densities on the mechanical properties of models. This simulation aids in verifying the desired mechanical behavior of the overall 3-D object and pinpointing potential stress points prior to manufacturing.

Given that NinjaFlex exhibits elastic-plastic characteristics with linear hardening in its plastic phase [66], we employed a bilinear elastic–plastic material model for our simulations. Forces between 0 to 10N were applied to the deformable side of the infill, which was fixed at its opposite end.

While we conducted simulations for 14 different configurations, space constraints limited the detailed presentation of all results. Some typical force–strain variations are illustrated in Fig. 4. The conducted result includes 11 standard 2-D and 3-D designs and three isolated 2-D patterns, i.e., concentric, cross, and grid patterns. All of the isolated 2-D patterns are paired with a bottom layer, otherwise, the simulation will not go through successfully because of isolated regions. The Grid pattern here was used as a baseline for isolated 2-D patterns.

For clarity, linear fits were added to all the scatter plots, which display data up to a 2-mm strain and 10 N force. To evaluate the overall performance across different parameters, we have combined all the 2-D and 3-D data in Fig. 5. This figure plots infill patterns against Young's modulus, with infill densities differentiated by shading intensities: darkest for 80%, middle lightness for 60%, and lightest for 40%. A distinct white bar marks the 60% density for clarity. Young's modulus, denoted as E, serves as a metric to gauge a material's resistance to elastic deformation. It is computed from the gradient of the linear fit in the scatter plot (Fig. 4), taking into account the dimensions of the 10 mm cubes.

From Fig. 5, isolated 2-D patterns emerge as the softest and most deformable architectures. Even with an added bottom layer, their compressibility surpasses other designs, closely followed by the 40% Grid infill. According to Fan and Coutrix [67], materials or structures with a Young's modulus between 10^4Pa and 10^6Pa are classified as soft structures. The parameters that fall within this range include most of 40% patterns except gyroid and cubic for 3-D infills, and cross, concentric, and grid patterns with 40% and 60% densities for 2-D infills. 40% or under might be the triggering infill density that turns the structure into the region of soft

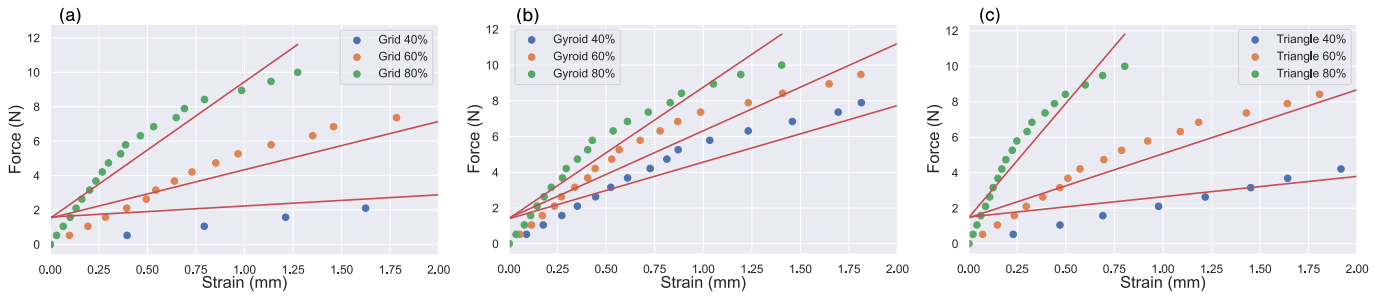

Fig. 4. Force-strain simulation result. (a) Grid. (b) Gyroid. (c) Triangle infill patterns with associated fit lines.

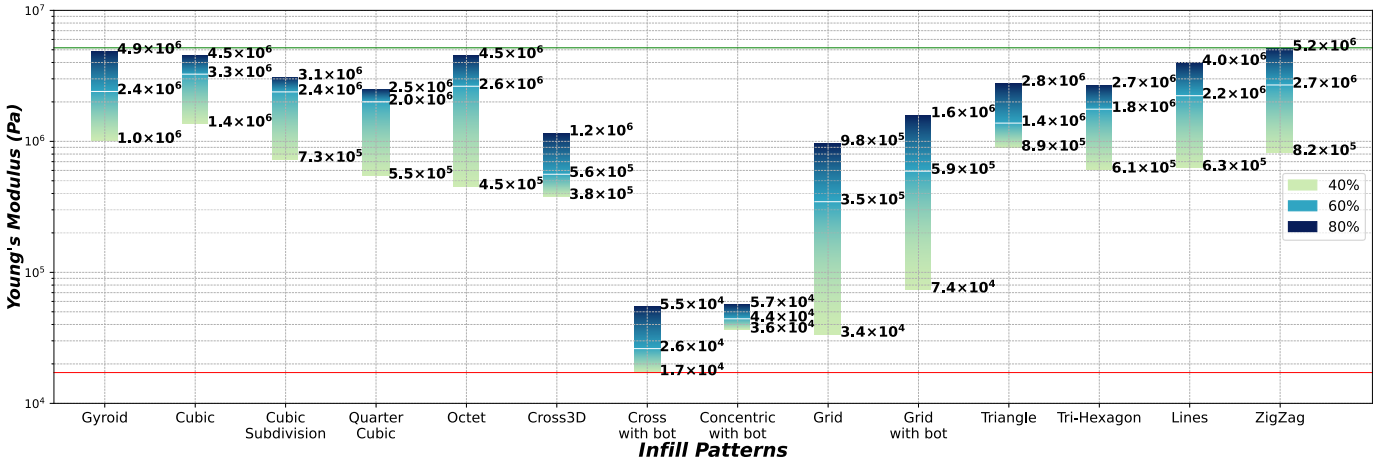

Fig. 5. Compression simulation results: Comparison of Young's modulus across infill patterns on a logarithmic scale.

structure. Notably, patterns with bottom layers need careful consideration, as they are not technically independent infills.

Among 3-D infills, the Gyroid pattern is the stiffest, while ZigZag stands out among the 14 models tested. Their stiffness makes them apt for detecting higher pressure. A general trend observed is that increased infill densities correlate with enhanced stiffness. The Grid patterns display the largest dynamic range logarithmically, while Zigzag patterns excel linearly. The Gyroid pattern, inherently rigid, is ideal for omnidirectional sensing, whereas Zigzag is tailored for unidirectional sensing. Conclusively, for dynamic range adjustments, we recommend using the Gyroid or Zigzag at the 10^6Pa scale, Grid at 10^5Pa, and Cross at 10^4Pa.

Utilizing the bar chart in Fig. 6(a), we contrasted the peak compressive stress across diverse infill patterns and densities. The equivalent stress map [Fig. 6(b)–(j)] after the compression is also used to identify the weak locations in the infill bearing a higher stress level. Shown patterns include conventional 2-D designs ("Grid," "Triangle," "ZigZag,") isolated 2-D patterns ("Cross with Bottom," "Concentric With Bottom," "Grid with Bottom" as control), and 3-D infills ("Gyroid," "Cross3D," "Cubic Subdivision") across 40%, 60%, and 80% densities. The maximum stress levels of each pattern are represented via individual bars, with separate bars for compressive stresses at each density level. The x-axis lists the infill patterns, while the y-axis quantifies the stress on a logarithmic scale.

Fig. 6(a) reveals that under the same pressure, the Zigzag and Cross patterns experience the lowest and highest maximum stress, respectively, among all 2-D and 3-D patterns. The Gyroid and Cross3D patterns show the least and most stress within the 3-D patterns. Fig. 6(b)–(j) further demonstrates that 3-D infill patterns [Fig. 6(h)–(j)] distribute pressure more uniformly than 2-D patterns [Fig. 6(b)–(g)], leading to fewer instances of extreme stress at specific points. This uniform distribution suggests that 2-D patterns, prone to stress concentration, are more susceptible to long-term wear and aging compared to 3-D patterns. Overall, the Zigzag pattern [Fig. 6(d)], with its lower stress, suits sensors needing a tougher structure for unidirectional deformation. Conversely, the Gyroid pattern [Fig. 6(j)], due to its durability and ability to handle omnidirectional stress, is better suited for long-lasting, versatile applications. The Cross, Concentric, and Cross3D patterns [Fig. 6(e)–(g)], noted for their high deformability at pressures below 10^5Pa, offer enhanced sensitivity for softer architectures but may face challenges in long-term durability.

B. Real Compression Result

To compare real compression tests with simulation results, we 3-D printed 10-mm cubes using three infill patterns: Gyroid, Grid, and Triangle, each at densities of 40%, 60%, and 80%. The Gyroid pattern and Grid pattern are the overall stiffest and softest among 3-D patterns and standard 2-D patterns, respectively. And the Triangle offers a more stable structure with minimal logarithmic variability in standard 2-D infills. We used the Makergear M3-ID 3-D printer.[4] Following

[4]https://makergear.com/products/m3-id

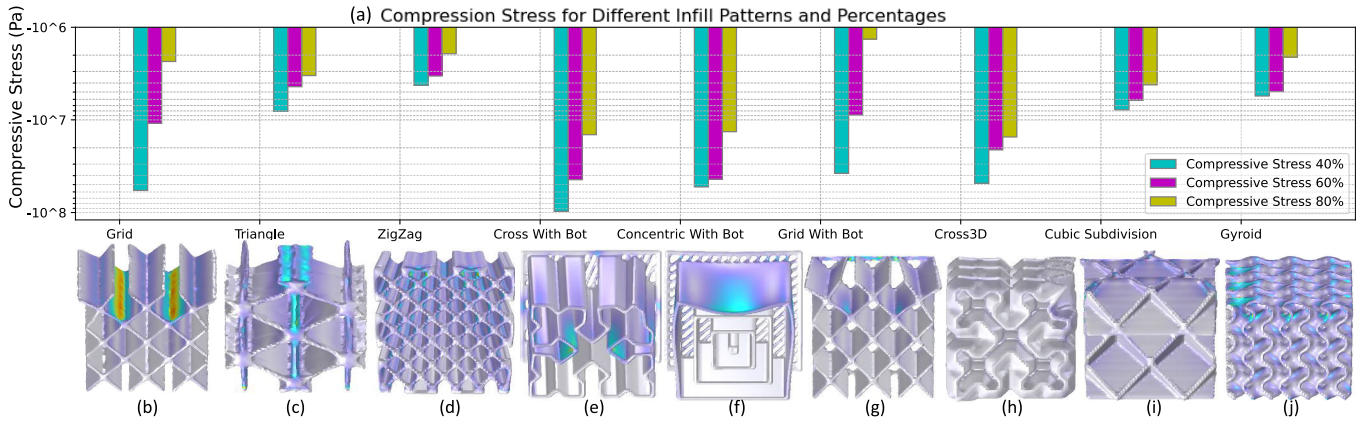

Fig. 6. (a) Maximum compressive stress under an applied force. (b)–(j) Stress simulation maps for each pattern with 40% density. (b) Grid. (c) Triangle. (d) ZigZag. (e) Cross with Bot. (f) Concentric with Bot. (g) Grid with Bot. (h) Cross3D. (i) Cubic Subdivision. (j) Gyroid.

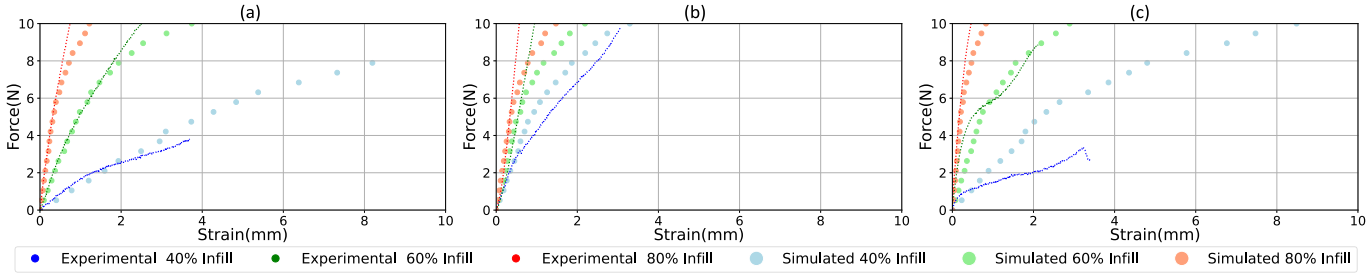

Fig. 7. Comparison of simulated and experimental data for force and strain. (a) Grid. (b) Gyroid. (c) Triangle patterns.

printing, we performed 20 rounds of compression tests on each sample using an FGD-50 force gauge.[5]

The force–displacement data are plotted in Fig. 7 to provide insights into the mechanical behavior of various infill parameters. Fig. 7(a)–(c) indicates that regardless of the infill pattern, a greater infill density makes the infill stiffer, aligning with the simulation results. From the three plots, the Gyroid pattern emerges as the stiffest, suitable for enduring substantial compressive loads. In contrast, the Grid pattern, with its higher compressibility and linear response, is optimal for significant deformation under minimal loads. These characteristics of the different infill patterns, along with variations in infill density, can be effectively used in designing soft sensors.

In Fig. 7(a)–(c), as represented by different colors and sizes of points in the graph, we observed close alignment between simulated and experimental data in Grid and Gyroid patterns at 60% and 80% infill densities. However, the Triangle pattern displayed minor deviations at 60% but showed improved alignment at 80%. At a lower infill density of 40%, the differences in pattern performance became significantly more evident. This increased divergence can likely be linked to printing challenges, such as overhangs or the formation of hollow areas. These anomalies are often a result of printer under-extrusion or over-extrusion, leading to inconsistencies in the final print. Consequently, for structures where a low Young's modulus is desirable, opting for higher infill densities is advisable to ensure more reliable and consistent print outcomes.

V. Customizable Pressure Sensor Design Tool

In this section, we mainly discuss the functionality and benefits of our design tool. As shown in Fig. 8, the findings beforehand are integrated into our tool to provide customizable softness architectures for user applications, with recommended profiles to increase the success rate of printing.

As shown in Fig. 8(a), we provide two force profile options and a slider for selecting the material's Young's modulus. For force selection, users can choose based on preference, e.g., 2-D infill for unidirectional force and 3-D infill for omnidirectional force. The default option is unidirectional force.

According to the classification by Fan and Coutrix [67], materials ranging from 10^4Pa to 10^6Pa are considered soft, while those exceeding 10^6Pa are deemed hard. Therefore, we offer a Young's Modulus range of 10^4Pa to 10^7Pa, allowing users to choose between soft and hard applications, which is consistent with our findings as well. For a specific Young's Modulus, there might be multiple choices. For example, both 80% Grid pattern and 40% Gyroid pattern may have similar Young's Modulus. Meanwhile, our simulation and experimental results show that higher infill density matches the theoretical results better and more predictable. To streamline the choices, the design tool typically advises users to select the one with higher infill density. Furthermore, We also display application images at the bottom right, corresponding to the selected Young's Modulus, to guide users in their design choices.

[5]https://www.testequip.com.au/digital-force-gauge-starr-instruments-fgd-series

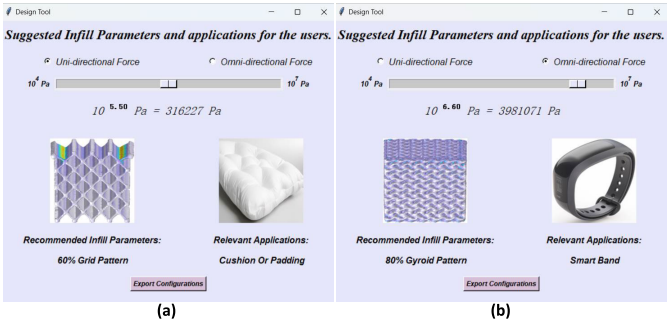

Fig. 8. Design tool overview: Recommended infill settings and associated applications for scenarios (a) and (b).

Through this step-by-step filtering and condition-matching process, we can achieve an optimal alignment between Young's Modulus and the ideal architecture, making it more user-friendly. Furthermore, our design tool can export a profile in CSV format based on user requirements, which can be imported into slicing tool files, such as Cura, for precise customization. This enhances the user experience of the tool.

VI. Exemplar Applications

Mechanical properties of pressure sensors have to aid its sensing methodology and match the form of application. It is used in order to provide sensitive and accurate readings [68]. In this section, we describe three application scenarios for pressure sensors made with different infill architectures, a cup holder to sense the remaining liquid level in the cup, an arm strap to sense the bending angle of the elbow, and a slipper sole to track the movement.

We made use of our analysis of different infill parameters to select the most suitable infill architecture for each pressure or deformable sensor. We first identified the target pressure range for each application based on empirical studies. Second, we selected the infill parameters that deform in a suitable range with the help of the design tool. This allows us to achieve high sensitivity and accuracy in the sensor readings. Also, we focused on maintaining a maximum allowable deformation to suit the application and avoid failure in the architecture. If multiple options are available for the target range, we will follow the recommendation from the design tool, i.e., the pattern with higher infill density.

In the slicing tool, we used fixed infill orientation. Therefore, we rotated the models for vertical placement on the bed [see Fig. 9(a) and (b)]. Midway through printing, we embedded a disk magnet [Fig. 9(d)] into unfinished 3-D prints. Consequently, when force is applied on top, the TI-DRV5055A1EDBZRQ1 hall-effect sensor [Fig. 9(c)] can detect magnetic field changes. The sensor output corresponds to the infill architecture's deformation since it is proportional to the distance between the Hall-effect sensor and the magnet.

A. Cup Holder

Proper hydration is essential for health. We printed a cup holder that detects the water level and prompts for refills.

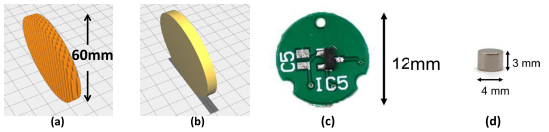

Fig. 9. (a) Vertical orientation of a model as printed in slicing tool. (b) Vertical orientation of an infill pattern model. (c) Custom PCB with hall-effect sensor. (d) Eclipse N802RS 4 × 3-mm Neodymium Magnet.

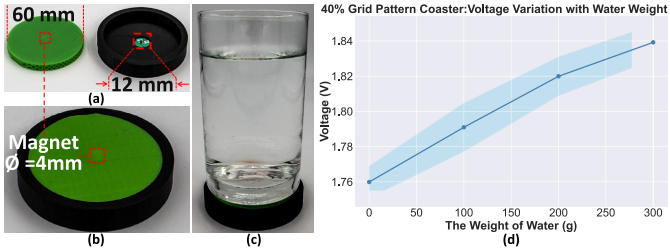

Fig. 10. (a) Three-dimensional printed cup holder. (b) Placement of the hall effect sensor inside the grid infill. (c) Water glass placed on the cup holder. (d) Coaster sensor voltage output variation with the weight of water.

A 40% density Grid pattern is designed in the cup holder. As the water level rises, the weight compresses the infill, increasing the sensor's reading. This enables measuring the water level.

Fig. 10(d) presents the sensor outputs obtained for four different amounts of water, empty, 100, 200, and 300 g. It shows that the output of the sensor increases when the water level is increased. This is due to higher weight results in a higher displacement of the infill.

B. Arm Strap

The elbow joint bending angle is important information for body motion tracking. We developed an arm strap with an embedded soft sensor to measure the bending angle of the arm joint. We have 3-D printed a strap to be worn on the upper arm. This strap [Fig. 11(a)] has a small bubble-like section, made by placing a Gyroid infill with 40% density between a magnet and a hall-effect sensor. When worn on the biceps, the sensor detects muscle movement as the biceps contract and relax when the elbow bends. This change in muscle shape causes variations in the sensor's output.

Fig. 11(e) displays the sensor pressure fluctuations over time during periodic arm joint bending (Fig. 11(b)–(d). Peaks indicate joint bending, while troughs represent the release of the arm joint. As shown in Fig. 11(e), the output remains relatively stable over time without any noticeable hysteresis, indicating the reliability of magnetic sensing.

C. Slipper Insole

Daily step counting is increasingly recognized for its fitness mode, from calculating burned calories to gauging walking pace. It plays a pivotal role in detecting falls [69], assisting in medical rehabilitation [70], and enhancing augmented reality footwear experience [71]. Research by Hessert et al. [72] highlights a significant foot pressure concentration on the heel and toes during ambulation. Leveraging this, we integrated

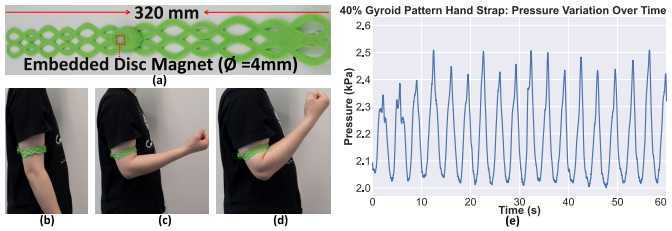

Fig. 11. (a) Hand strap featuring an embedded soft sensor. (b) Relaxed arm. (c) Partially bent arm. (d) Fully bent arm. (e) Hand strap sensor pressure variation over time.

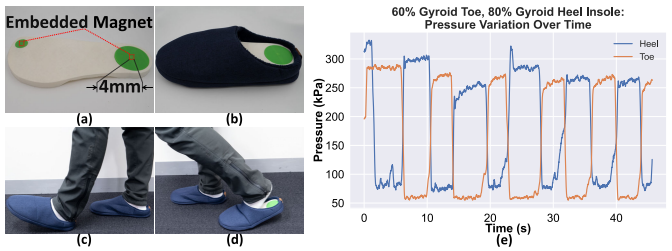

Fig. 12. Slipper insole with toe and heel sensors. (a) Sensor locations. (b) Inside shoe placement. (c) and (d) Heel and toe pressure application. (e) Insole sensor pressure over time.

two pressure sensors into a slipper sole, positioned at the heel and toes as depicted in Fig. 12(a). Relying on Hessert's findings [72] and our design tool, the heel sensor utilizes an 80% Gyroid infill architecture, whereas the toe sensor adopts a 60% Gyroid infill.

As we walk, the heel-to-toe contact occurs in an alternating sequence. Monitoring outputs from both sensors enables step counting and the detection of irregular movements. Fig. 12(e) shows this weight transition from heel to toe when walking.

VII. Discussion and Limitations

In this section, we discuss our observations on the proposed approach and potential application scenarios along with the key limitations and possible future directions.

A. Discussion

In this article, we emphasize the importance of infill manipulation in shaping the mechanical properties of 3-D printed sensors. The parameters of infill directly impact properties like Young's Modulus that further influence the force–strain behaviors. As infill density increases, stiffness also rises. Specific infill patterns can then further refine the mechanical response. We recommend Cross patterns for Young's modulus around 10^4Pa, Grid patterns for 10^5Pa, Triangle or Cross3D patterns for 10^6Pa, and Zigzag or Gyroid patterns for 10^7Pa. The choice of patterns depends on the user's needs. For a given Young's modulus, patterns with denser infills are preferred due to their predictable simulation results and the reliability of the printed samples.

The proposed adjustable infill in 3-D printing provides various customizable applications that may benefit the community. In smart homes and IoT contexts, rigid sensors can function as furniture, while softer ones can be seamlessly embedded in items like cushions or pillows. In robotics, sensors can be customized based on environmental interactions. The sports sector can embed these sensors in gear, such as footwear, for enhanced gait analysis. The gaming industry can offer personalized feedback through user-tailored peripherals. Overall, infill modifications in 3-D printing present opportunities for customized solutions across various sectors.

B. Limitations and Future Work

Despite the promising results of our research, there exist several limitations that should be addressed in future work.

1) Other Infill Configurations: In this article, we examined 14 infill patterns, including Gyroid, the only bio-inspired 3-D infill used [35]. Other bio-inspired 3-D patterns like Schwarz P and Schwarz D were not tested because they are not available in Cura.[6] And certain 2-D patterns like Honeycomb and Hilbert Curve are not currently available in Cura as well. These patterns can potentially be added to Cura from their GitHub repository and may be topics for future investigation.[7]

While using infills inside objects, we have used a fixed infill density throughout the body. Future research can consider varying the infill densities at different locations of the object to equalize the stress level throughout the body. This enables us to improve the strength-to-weight ratio and strengthen locations with higher stress.

2) Limited Types of Deformation: We focused on forces applied perpendicularly to the sensor. Future analysis could explore other deformations like shear, twisting, pinching, or one-end pressing using data-driven modeling [73], [74], [75], [76], [77]. Meanwhile, materials have different properties under tensile and compressive loads. These aspects could lead to a more insightful understanding of unevenly distributed force responses.

3) Interference of Magnetic Fields: External magnetic fields can interfere with our measurements, leading to data inconsistencies, especially in environments with variable magnetic fields. To mitigate this, future research could investigate using ferromagnetic 3-D printing filaments for electromagnetic shielding [78]. This approach involves printing the infill walls with a ferromagnetic material, which can absorb or redirect magnetic interference. It could involve a trade-off between the structural rigidity (density) of the wall and its shielding effectiveness [79]. Further research is needed to optimize this balance and to develop more effective shielding techniques that do not compromise the structural integrity of the prints.

VIII. Conclusion

In this work, we introduce a novel approach for fabricating customizable pressure sensors by tuning the infill characteristics of flexible 3-D prints, addressing the need for precise sensing solutions in various applications. Our method, grounded in both computational simulations and empirical data, systematically alters Young's modulus through infill parameters, enabling the creation of sensors with tailored responses. We identified optimal infill patterns for specific

[6]https://kenbrakke.com/evolver/examples/periodic/periodic.html
[7]https://all3dp.com/2/get-cura-honeycomb-infill

applications and found that higher infill densities were found to align more closely with theoretical predictions. Additionally, we developed a design tool that facilitates precise modification of sensor sensitivity and dynamic range and suggests parameters to enhance printing quality. Demonstrating the versatility of our method, we fabricated sensors for three distinct applications, each with unique sensing needs. This innovative approach significantly advances the field of customizable pressure sensor development, offering enhanced precision and flexibility for practical and innovative applications.

Acknowledgment

The authors would like to acknowledge Nisal Menuka Gamage and Thejan Elankayer for their key early contributions to this project. They thank all our user study participants and anonymous reviewers for their valuable feedback.

References

[1] D. Tetteroo et al., "Lessons learnt from deploying an end-user development platform for physical rehabilitation," in *Proc. 33rd Annu. ACM Conf. Hum. Factors Comput. Syst.*, Apr. 2015, pp. 4133–4142.

[2] G. Wang et al., "ThermoFit: Thermoforming smart orthoses via metamaterial structures for body-fitting and component-adjusting," *Proc. ACM Interact., Mobile, Wearable Ubiquitous Technol.*, vol. 7, no. 1, pp. 1–27, Mar. 2023.

[3] K. Marky, M. Schmitz, V. Zimmermann, M. Herbers, K. Kunze, and M. Mühlhäuser, "3D-auth: Two-factor authentication with personalized 3D-printed items," in *Proc. CHI Conf. Hum. Factors Comput. Syst.*, New York, NY, USA, Apr. 2020, pp. 1–12.

[4] R. Colella and L. Catarinucci, "Wearable UHF RFID sensor-tag based on customized 3D-printed antenna substrates," *IEEE Sensors J.*, vol. 18, no. 21, pp. 8789–8795, Nov. 2018.

[5] Y.-J. Lin et al., "FoodFab: Creating food perception illusions using food 3D printing," in *Proc. CHI Conf. Human Factors Comput. Syst.*, New York, NY, USA, Apr. 2020, pp. 1–13.

[6] M. Schmitz, F. Müller, M. Mühlhäuser, J. Riemann, and H. V. V. Le, "Itsy-bits: Fabrication and recognition of 3D-printed tangibles with small footprints on capacitive touchscreens," in *Proc. CHI Conf. Hum. Factors Comput. Syst.*, May 2021, pp. 1–12.

[7] Y. Tao et al., "Demonstrating thermorph: Democratizing 4D printing of self-folding materials and interfaces," in *Proc. Extended Abstr. CHI Conf. Hum. Factors Comput. Syst.*, New York, NY, USA, Apr. 2018, pp. 1–12.

[8] M. Schmitz, J. Steimle, J. Huber, N. Dezfuli, and M. Mühlhäuser, "Flexibles: Deformation-aware 3D-printed tangibles for capacitive touchscreens," in *Proc. CHI Conf. Hum. Factors Comput. Syst.*, New York, NY, USA, May 2017, pp. 1001–1014.

[9] J. Gong, O. Seow, C. Honnet, J. Forman, and S. Mueller, "MetaSense: Integrating sensing capabilities into mechanical metamaterial," in *Proc. 34th Annu. ACM Symp. User Interface Softw. Technol.*, Oct. 2021, pp. 1063–1073.

[10] V. Iyer, J. Chan, and S. Gollakota, "3D printing wireless connected objects," *ACM Trans. Graph.*, vol. 36, no. 6, pp. 1–13, Dec. 2017.

[11] M. Schmitz, M. Stitz, F. Müller, M. Funk, and M. Mühlhäuser, "./trilaterate: A fabrication pipeline to design and 3D print hover-, touch-, and force-sensitive objects," in *Proc. CHI Conf. Hum. Factors Comput. Syst.*, May 2019, pp. 1–13.

[12] M. Ntagios and R. Dahiya, "3D printed soft and flexible insole with intrinsic pressure sensing capability," *IEEE Sensors J.*, vol. 23, no. 20, pp. 23995–24003, Oct. 2023.

[13] M. L. Rivera, M. Moukperian, D. Ashbrook, J. Mankoff, and S. E. Hudson, "Stretching the bounds of 3D printing with embedded textiles," in *Proc. CHI Conf. Hum. Factors Comput. Syst.*, New York, NY, USA, May 2017, pp. 497–508.

[14] H. Y. Jeong et al., "3D printing of twisting and rotational bistable structures with tuning elements," *Sci. Rep.*, vol. 9, no. 1, p. 324, Jan. 2019.

[15] Z. Yan and H. Peng, "FabHydro: Printing interactive hydraulic devices with an affordable SLA 3D printer," in *Proc. 34th Annu. ACM Symp. User Interface Softw. Technol.*, New York, NY, USA, Oct. 2021, pp. 298–311.

[16] O. Ozioko, H. Nassar, and R. Dahiya, "3D printed interdigitated capacitor based tilt sensor," *IEEE Sensors J.*, vol. 21, no. 23, pp. 26252–26260, Dec. 2021.

[17] C. Hong, Y. Zhang, Z. Lu, and Z. Yin, "A FBG tilt sensor fabricated using 3D printing technique for monitoring ground movement," *IEEE Sensors J.*, vol. 19, no. 15, pp. 6392–6399, Aug. 2019.

[18] R. Chirila, M. Ntagios, and R. Dahiya, "3D printed wearable exoskeleton human-machine interfacing device," in *Proc. IEEE Sensors*, Oct. 2020, pp. 1–4.

[19] W. Yang, Y. Liu, W. Xu, and H.-Y. Nie, "Design and fabrication of flexible capacitive sensor with cellular structured dielectric layer via 3D printing," *IEEE Sensors J.*, vol. 21, no. 9, pp. 10473–10482, May 2021.

[20] H. Takahashi and J. Kim, "3D printed fabric: Techniques for design and 3D weaving programmable textiles," in *Proc. 32nd Annu. ACM Symp. User Interface Softw. Technol.*, New York, NY, USA, Oct. 2019, pp. 43–51.

[21] W. Wang et al., "Novel coil transducer induced thermoacoustic detection of rail internal defects towards intelligent processing," *IEEE Trans. Ind. Electron.*, vol. 71, no. 2, pp. 2100–2111, Feb. 2024.

[22] E. Chau, J. Yu, C. Goncu, and A. Withana, "Composite line designs and accuracy measurements for tactile line tracing on touch surfaces," *Proc. ACM Hum.-Comput. Interact.*, vol. 5, pp. 1–17, Nov. 2021.

[23] G. Wang et al., "MorphingCircuit: An integrated design, simulation, and fabrication workflow for self-morphing electronics," *Proc. ACM Interact., Mobile, Wearable Ubiquitous Technol.*, vol. 4, no. 4, pp. 1–26, Dec. 2020.

[24] P. Punpongsanon, X. Wen, D. S. Kim, and S. Mueller, "ColorMod: Recoloring 3D printed objects using photochromic inks," in *Proc. CHI Conf. Hum. Factors Comput. Syst.*, New York, NY, USA, Apr. 2018, pp. 1–12.

[25] Y. Jin, I. Qamar, M. Wessely, and S. Mueller, "Photo-chromeleon: Re-programmable multi-color textures using photochromic dyes," in *Proc. ACM SIGGRAPH Emerg. Technol.*, Aug. 2020, pp. 1–2.

[26] T. Yu et al., "Thermotion: Design and fabrication of thermofluidic composites for animation effects on object surfaces," in *Proc. CHI Conf. Hum. Factors Comput. Syst. (CHI)*. New York, NY, USA: Association for Computing Machinery, 2023, pp. 1–19, Paper 425. [Online]. Available: https://doi.org/10.1145/3544548.3580743

[27] D. C. Corbett et al., "Thermofluidic heat exchangers for actuation of transcription in artificial tissues," *Sci. Adv.*, vol. 6, no. 40, Oct. 2020, Art. no. eabb9062.

[28] E. M. Palmero et al., "Magnetic-polymer composites for bonding and 3D printing of permanent magnets," *IEEE Trans. Magn.*, vol. 55, no. 2, pp. 1–4, Feb. 2019.

[29] X. Cao, S. Xuan, S. Sun, Z. Xu, J. Li, and X. Gong, "3D printing magnetic actuators for biomimetic applications," *ACS Appl. Mater. Interface*, vol. 13, no. 25, pp. 30127–30136, Jun. 2021.

[30] W. Wang et al., "MRC-based double figure-of-eight coil sensor system with triple-mode operation capability for biomedical applications," *IEEE Sensors J.*, vol. 21, no. 13, pp. 14491–14502, Jul. 2021.

[31] Z. H. Nick, C. E. Tabor, and R. L. Harne, "Liquid metal microchannels as digital sensors in mechanical metamaterials," *Extreme Mech. Lett.*, vol. 40, Oct. 2020, Art. no. 100871.

[32] C. El Helou, P. R. Buskohl, C. E. Tabor, and R. L. Harne, "Digital logic gates in soft, conductive mechanical metamaterials," *Nature Commun.*, vol. 12, no. 1, pp. 1–8, Mar. 2021.

[33] M. Rismalia, S. C. Hidajat, I. G. R. Permana, B. Hadisujoto, M. Muslimin, and F. Triawan, "Infill pattern and density effects on the tensile properties of 3D printed PLA material," *J. Phys., Conf. Ser.*, vol. 1402, no. 4, Dec. 2019, Art. no. 044041.

[34] B. Pernet, J. K. Nagel, and H. Zhang, "Compressive strength assessment of 3D printing infill patterns," *Proc. CIRP*, vol. 105, pp. 682–687, Jan. 2022.

[35] J. Podroužek, M. Marcon, K. Ninčević, and R. Wan-Wendner, "Bio-inspired 3D infill patterns for additive manufacturing and structural applications," *Materials*, vol. 12, no. 3, p. 499, Feb. 2019.

[36] S. Olberding, S. Soto Ortega, K. Hildebrandt, and J. Steimle, "Foldio: Digital fabrication of interactive and shape-changing objects with foldable printed electronics," in *Proc. 28th Annu. ACM Symp. User Interface Softw. Technol.* Bedford, MA, USA: Digital, Nov. 2015, pp. 223–232.

[37] J. Yamaoka et al., "FoldTronics: Creating 3D objects with integrated electronics using foldable honeycomb structures," in *Proc. CHI Conf. Hum. Factors Comput. Syst.*, May 2019, pp. 1–14.

[38] M. Weigel, T. Lu, G. Bailly, A. Oulasvirta, C. Majidi, and J. Steimle, "ISkin: Flexible, stretchable and visually customizable on-body touch sensors for mobile computing," in *Proc. 33rd Annu. ACM Conf. Hum. Factors Comput. Syst.*, Apr. 2015, pp. 2991–3000.

[39] H.-L. Kao, C. Holz, A. Roseway, A. Calvo, and C. Schmandt, "DuoSkin: Rapidly prototyping on-skin user interfaces using skin-friendly materials," in *Proc. ACM Int. Symp. Wearable Comput.*, New York, NY, USA, Sep. 2016, pp. 16–23.

[40] A. Ion et al., "Metamaterial mechanisms," in *Proc. 29th Annu. Symp. User Interface Softw. Technol.*, 2016, pp. 529–539.

[41] S. S.-R. Lin, N. M. Gamage, K. Herath, and A. Withana, "MyoSpring: 3D printing mechanomyographic sensors for subtle finger gesture recognition," in *Proc. 16th Int. Conf. Tangible, Embedded, Embodied Interact.*, Feb. 2022, pp. 1–13.

[42] J.-H. Pu et al., "A strain localization directed crack control strategy for designing MXene-based customizable sensitivity and sensing range strain sensors for full-range human motion monitoring," *Nano Energy*, vol. 74, Aug. 2020, Art. no. 104814.

[43] Z. Xu et al., "A flexible pressure sensor with highly customizable sensitivity and linearity via positive design of microhierarchical structures with a hyperelastic model," *Microsyst. Nanoeng.*, vol. 9, no. 1, p. 5, Jan. 2023.

[44] L. Wu et al., "Customizable self-powered pressure sensor based on piezo-transmittance of tilted structures," *Nano Energy*, vol. 109, May 2023, Art. no. 108299.

[45] A. G. Leal-Junior, C. Marques, M. R. N. Ribeiro, M. J. Pontes, and A. Frizera, "FBG-embedded 3-D printed ABS sensing pads: The impact of infill density on sensitivity and dynamic range in force sensors," *IEEE Sensors J.*, vol. 18, no. 20, pp. 8381–8388, Oct. 2018.

[46] D. L. Presti et al., "The effect of infill pattern and density on the response of 3-D-printed sensors based on FBG technology," *IEEE Sensors J.*, vol. 22, no. 20, pp. 19357–19365, Oct. 2022.

[47] A. Z. Stefanov, L. D. Živanov, M. G. Kisic, and A. B. Menicanin, "Fully FFF-printed capacitive displacement sensor based on graphene/PLA composite and thermoplastic elastomer filaments," *IEEE Sensors J.*, vol. 22, no. 11, pp. 10437–10445, Jun. 2022.

[48] M. Samykano, S. K. Selvamani, K. Kadirgama, W. K. Ngui, G. Kanagaraj, and K. Sudhakar, "Mechanical property of FDM printed ABS: Influence of printing parameters," *Int. J. Adv. Manuf. Technol.*, vol. 102, nos. 9–12, pp. 2779–2796, Jun. 2019.

[49] E. Hobert, "3D printed flexible fingertip strain sensor," B.S. thesis, Dept. Elect. Eng., Math. Comput. Sci., Univ. Twente, Enschede, The Netherlands, 2017.

[50] M. Bächer et al., "DefSense: Computational design of customized deformable input devices," in *Proc. CHI Conf. Hum. Factors Comput. Syst.*, New York, NY, USA, May 2016, pp. 3806–3816.

[51] A. Oliveri, M. Maselli, M. Lodi, M. Storace, and M. Cianchetti, "Model-based compensation of rate-dependent hysteresis in a piezoresistive strain sensor," *IEEE Trans. Ind. Electron.*, vol. 66, no. 10, pp. 8205–8213, Oct. 2019.

[52] L. Duan, D. R. D'hooge, and L. Cardon, "Recent progress on flexible and stretchable piezoresistive strain sensors: From design to application," *Prog. Mater. Sci.*, vol. 114, Oct. 2020, Art. no. 100617.

[53] A. Sharma et al., "SparseIMU: Computational design of sparse IMU layouts for sensing fine-grained finger microgestures," *ACM Trans. Comput.-Hum. Interact.*, vol. 30, no. 3, pp. 1–40, Jun. 2023.

[54] S. Majumder and M. J. Deen, "Wearable IMU-based system for real-time monitoring of lower-limb joints," *IEEE Sensors J.*, vol. 21, no. 6, pp. 8267–8275, Mar. 2021.

[55] M. Rana and V. Mittal, "Wearable sensors for real-time kinematics analysis in sports: A review," *IEEE Sensors J.*, vol. 21, no. 2, pp. 1187–1207, Jan. 2021.

[56] P. T. Smith, R. R. Vallance, and E. R. Marsh, "Correcting capacitive displacement measurements in metrology applications with cylindrical artifacts," *Precis. Eng.*, vol. 29, no. 3, pp. 324–335, Jul. 2005.

[57] D.-C. Wang, J.-C. Chou, S.-M. Wang, P.-L. Lu, and L.-P. Liao, "Application of a fringe capacitive sensor to small-distance measurement," *Jpn. J. Appl. Phys.*, vol. 42, pp. 5816–5820, Sep. 2003.

[58] J. McIntosh, P. Strohmeier, J. Knibbe, S. Boring, and K. Hornbæk, "Magnetips: Combining fingertip tracking and haptic feedback for around-device interaction," in *Proc. CHI Conf. Hum. Factors Comput. Syst.*, New York, NY, USA, May 2019, pp. 1–12.

[59] W. Wang, Q. Cao, and Y. Zheng, "Bandstop frequency-selective structures based on stepped-impedance loop resonators: Design, analysis, and measurement," *IEEE Trans. Antennas Propag.*, vol. 67, no. 2, pp. 1053–1064, Feb. 2019.

[60] W. Wang, S. Yang, Z. Fang, Q. Sun, Y. Chen, and Y. Zheng, "Compact dual-polarized wideband antenna with dual-/single-band shifting for microbase station applications," *IEEE Trans. Antennas Propag.*, vol. 69, no. 11, pp. 7323–7332, Nov. 2021.

[61] B. A. Kaidarova et al., "Flexible Hall sensor made of laser-scribed graphene," *NPJ Flexible Electron.*, vol. 5, no. 1, p. 2, Feb. 2021.

[62] W. Wang et al., "Wideband gain enhancement of MIMO antenna and its application in FMCW radar sensor integrated with CMOS-based transceiver chip for human respiratory monitoring," *IEEE Trans. Antennas Propag.*, vol. 71, no. 1, pp. 318–329, Jan. 2023.

[63] K. Kaphle, G. Karki, and A. Panthi, "Alternative approach for the calculation of magnetic field due to magnet for magnetic field visualization and evaluation," *J. Inst. Eng.*, vol. 15, no. 1, pp. 150–160, Feb. 2020.

[64] W. Wang et al., "Analysis and design of coil-based electromagnetic-induced thermoacoustic for rail internal-flaw inspection," *IEEE Trans. Intell. Transp. Syst.*, vol. 20, no. 7, pp. 2691–2702, Jul. 2019.

[65] R. Zou et al., "Isotropic and anisotropic elasticity and yielding of 3D printed material," *Compos. B, Eng.*, vol. 99, pp. 506–513, Aug. 2016.

[66] A. A. Pitaru et al., "Investigating commercial filaments for 3D printing of stiff and elastic constructs with ligament-like mechanics," *Micromachines*, vol. 11, no. 9, p. 846, Sep. 2020.

[67] Z. Fan and C. Coutrix, "Impact of softness on users' perception of curvature for future soft curvature-changing UIs," in *Proc. CHI Conf. Hum. Factors Comput. Syst. (CHI)*. New York, NY, USA: Association for Computing Machinery, 2023, pp. 1–19, Paper 747. [Online]. Available: https://doi.org/10.1145/3544548.3581179

[68] A. Nag, S. C. Mukhopadhyay, and J. Kosel, "Wearable flexible sensors: A review," *IEEE Sensors J.*, vol. 17, no. 13, pp. 3949–3960, Jul. 2017.

[69] L. Montanini, A. Del Campo, D. Perla, S. Spinsante, and E. Gambi, "A footwear-based methodology for fall detection," *IEEE Sensors J.*, vol. 18, no. 3, pp. 1233–1242, Feb. 2018.

[70] W. A. Kusuma, Z. Sari, H. Wibowo, S. Norhabibah, S. N. Ubay, and D. A. Fitriani, "Monitoring walking devices for calorie balance in patients with medical rehabilitation needs," in *Proc. 5th Int. Conf. Electr. Eng., Comput. Sci. Informat. (EECSI)*, Oct. 2018, pp. 460–463.

[71] D. Wittchen, V. Martinez-Missir, S. Mavali, N. Sabnis, C. N. Reed, and P. Strohmeier, "Designing interactive shoes for tactile augmented reality," in *Proc. Augmented Hum. Conf.*, Mar. 2023, pp. 1–14.

[72] M. J. Hessert, M. Vyas, J. Leach, K. Hu, L. A. Lipsitz, and V. Novak, "Foot pressure distribution during walking in young and old adults," *BMC Geriatrics*, vol. 5, no. 1, pp. 1–8, Dec. 2005.

[73] J. Liu et al., "Overfitting the data: Compact neural video delivery via content-aware feature modulation," in *Proc. IEEE/CVF Int. Conf. Comput. Vis. (ICCV)*, Oct. 2021, pp. 4631–4640.

[74] M. Li et al., "Instant: Semi-supervised learning with instance-dependent thresholds," in *Proc. 37th Conf. Neural Inf. Process. Syst. (NeurIPS)*, 2023.

[75] R. Lin, C. Yu, and T. Liu, "Eliminating catastrophic overfitting via abnormal adversarial examples regularization," in *Proc. 37th Conf. Neural Inf. Process. Syst. (NeurIPS)*, 2023.

[76] X. Xia et al., "Are anchor points really indispensable in label-noise learning?" in *Proc. Adv. Neural Inf. Process. Syst. (NeurIPS)*, 2019.

[77] X. Xia et al., "Part-dependent label noise: Towards instance-dependent label noise," in *Proc. Adv. Neural Inf. Process. Syst.*, 2020, pp. 7597–7610.

[78] K. P. M. Lee, T. Baum, R. Shanks, and F. Daver, "Electromagnetic interference shielding of 3D-printed graphene–polyamide-6 composites with 3D-printed morphology," *Additive Manuf.*, vol. 43, Jul. 2021, Art. no. 102020.

[79] H. Wang, S. Li, M. Liu, J. Li, and X. Zhou, "Review on shielding mechanism and structural design of electromagnetic interference shielding composites," *Macromolecular Mater. Eng.*, vol. 306, no. 6, Jun. 2021, Art. no. 2100032.